Navigation Algorithms for Formation Flying Missions

Paul J. Huxel[*] and Robert H. Bishop[†]

University of Texas, Austin, TX, 78712

The objective of the investigations is to develop navigation algorithms to support formation flying missions. In particular, we examine the advantages and concerns associated with the use of combinations of inertial and relative measurements, as well as address observability issues. In our analysis we consider the interaction between measurement types, update frequencies, and trajectory geometry and their cumulative impact on observability. Furthermore, we investigate how relative measurements affect inertial navigation in terms of algorithm performance.

I.   Introduction

As space exploration and space technologies advance, so do the ambition and complexity of space missions. In particular, the interest in formation flying missions is on the rise. Using innovative formations of multiple spacecraft, these missions attempt to accomplish what would be too costly our simply impossible using only one spacecraft. With missions ranging from small formations for remote sensing and mapping to elaborate formations acting as interferometers and telescopes, precise and accurate inertial navigation will be vital for success. Fortunately, although the increase in spacecraft creates a more complex mission, it also provides a measurement rich environment. For example, by using cross-link range measurements (between each spacecraft), a formation of p spacecraft provides $p(p-1)/2$ relative measurements. With so many measurements available the question becomes: Can relative measurements be used to increase inertial navigation accuracy (in terms of algorithm performance)? We will show that while the answer to this question is "yes," the inclusion of relative measurements is not yet without concerns and limitations.

The discussions leading up to this statement are presented as follows. First, the extended Kalman filter algorithm, which is used by all the simulations in this paper, is presented. The system and measurement models are also described within this section. The next section outlines the observability condition that is used to analyze each simulation. Finally, three simulation are outlined in detail and the results of each are presented.

II.   Extended Kalman Filter Algorithm

The basis of the navigation algorithms used in this study is the continuous-discrete extended Kalman filter (EKF) as found in Gelb.[1] The EKF algorithm equations use the following shorthand notations. First, (t) or $(\mathbf{x})$ denotes that a variable is a continuous function of t or $\mathbf{x}$, respectively. Second, the subscript k explicitly denotes that a variable is taken at the discrete time t_k. And third, the term $(-)$ denotes a variable immediately before a measurement update, while the term $(+)$ denotes a variable immediately after

---

[*]Ph.D. Candidate and Research Assistant, Aerospace Engineering and Engineering Mechanics, 201 E. 24th St., WRW 219B, 1 University Station, C0600.

[†]Professor and Chairman, Aerospace Engineering and Engineering Mechanics, 201 E. 24th St., WRW 219B, 1 University Station, C0600 and AIAA Associate Fellow.

2nd International Symposium on Formation Flying Missions and Technologies

a measurement update. When variables are used outside of the algorithm equations these terms are dropped for convenience (so long as the context does not cause ambiguity).

A.   System and Measurement Models

The general continuous time (t) system model is setup as follows

$$\dot{\mathbf{x}}(t) = \mathbf{f}(\mathbf{x}(t), t) + \mathbf{w}(t) \qquad , \qquad \mathbf{w}(t) \sim N(\mathbf{0}, \mathbf{Q}_{spec}) \tag{1}$$

where $\mathbf{x}$ is the state vector and $\mathbf{w}$ is Gaussian white noise with covariance defined by the spectral density matrix $\mathbf{Q}_{spec}$. Like the state vector, the vector $\mathbf{f}$, which describes the dynamic model of the time derivative of the state $(\dot{\mathbf{x}})$, is problem dependent. The simulations presented in Section IV use the state and dynamics defined in Eq. (2), which are the dynamics of the inertial restricted three body problem (centered at body 1 with the mass of all p spacecraft negligible).

$$\mathbf{x} = \begin{bmatrix} \mathbf{r}_1 \\ \mathbf{v}_1 \\ \vdots \\ \mathbf{r}_p \\ \mathbf{v}_p \end{bmatrix} \qquad , \qquad \mathbf{f} = \begin{bmatrix} \mathbf{v}_1 \\ \mathbf{g}_1 \\ \vdots \\ \mathbf{v}_p \\ \mathbf{g}_p \end{bmatrix} \qquad , \qquad \mathbf{g}_i = \ddot{\mathbf{r}}_i = -\mu_1 \frac{\mathbf{r}_i}{r_i{}^3} - \mu_2 \left(\frac{\mathbf{d}_i}{d_i{}^3} + \frac{\mathbf{r}_{b_2}}{r_{b_2}{}^3} \right) \tag{2}$$

In Eq. (2) $\mathbf{r}_i$ and $\mathbf{v}_i$ are the respective position and velocity vectors of spacecraft i relative to body 1, μ_j is the gravitational parameter of body j, $\mathbf{d}_i$ is the position vector from body 2 to spacecraft i $(\mathbf{d}_i = \mathbf{r}_i - \mathbf{r}_{b_2})$, and $\mathbf{r}_{b_2}$ is the position vector from body 1 to body 2.

Equation (3) shows the general discrete time (t_k) measurement model setup, where $\mathbf{z}$ is the measurement vector and $\boldsymbol{\nu}$ is Gaussian white noise with covariance defined by the measurement noise matrix $\mathbf{R}$.

$$\mathbf{z}_k = \mathbf{h}_k(\mathbf{x}_k) + \boldsymbol{\nu}_k \qquad , \qquad \boldsymbol{\nu}_k \sim N(\mathbf{0}, \mathbf{R}_k) \tag{3}$$

The vector $\mathbf{h}$, which describes the measurement model in terms of the state, is also problem dependent. In the simulations presented in Section IV $\mathbf{h}$ is composed of different combinations of tracking station range measurements (ρ_{ji})

$$\rho_{ji} = \|\boldsymbol{\rho}_{ji}\| \qquad , \qquad \boldsymbol{\rho}_{ji} = \mathbf{r}_i - \mathbf{r}_{s_j} \tag{4}$$

where $\mathbf{r}_{s_j}$ is the position vector from body 1 to station j, and cross-link range measurements between spacecraft (r_{ij})

$$r_{ij} = \|\mathbf{r}_{ij}\| \qquad , \qquad \mathbf{r}_{ij} = \mathbf{r}_j - \mathbf{r}_i \quad (j > i). \tag{5}$$

Finally, Eq. (6) defines the condition of initial state estimate vector $(\hat{\mathbf{x}}_0)$, which has an initial uncertainty defined by the initial state error covariance matrix $\mathbf{P}_0$,

$$\mathbf{x}(0) \sim N(\hat{\mathbf{x}}_0, \mathbf{P}_0) \qquad , \qquad E\left[\mathbf{w}(t)\boldsymbol{\nu}_k^T\right] = 0 \quad \forall \quad t, k \tag{6}$$

as well as the condition that the system model noise $(\mathbf{w})$ and the measurement model noise $(\boldsymbol{\nu})$ are uncorrelated. The state error $(\mathbf{e})$ is defined as the difference between the state estimate and the true state $(\mathbf{e} = \hat{\mathbf{x}} - \mathbf{x})$.

B.   Dynamic Coefficient and Measurement Sensitivity Matrices

With the models now defined, the EKF requires partial derivatives of these models with respect to the state, as defined in Eq. (7).

$$\mathbf{F}_k = \left. \frac{\partial \mathbf{f}}{\partial \mathbf{x}} \right|_{\mathbf{x} = \hat{\mathbf{x}}(t_k)} \qquad , \qquad \mathbf{H}_k = \left. \frac{\partial \mathbf{h}}{\partial \mathbf{x}} \right|_{\mathbf{x} = \hat{\mathbf{x}}_k(-)} \tag{7}$$

Applying the definition for the dynamic coefficient matrix ($\mathbf{F}$) to Eq. (2) results in the following

$$\mathbf{F} = \begin{bmatrix} \mathbf{F}_1 & \mathbf{0} & \mathbf{0} \\ \mathbf{0} & \ddots & \mathbf{0} \\ \mathbf{0} & \mathbf{0} & \mathbf{F}_p \end{bmatrix} \quad , \quad \mathbf{F}_i = \begin{bmatrix} \mathbf{0} & \mathbf{I} \\ \mathbf{G}_i & \mathbf{0} \end{bmatrix} \tag{8}$$

where

$$\mathbf{G}_i = \frac{\partial \mathbf{g}_i}{\partial \mathbf{r}_i} = \frac{\mu_1}{r_i{}^5}\left(3\mathbf{r}_i\mathbf{r}_i{}^T - r_i{}^2\mathbf{I}\right) + \frac{\mu_1}{d_i{}^5}\left(3\mathbf{d}_i\mathbf{d}_i{}^T - d_i{}^2\mathbf{I}\right) \tag{9}$$

and $\mathbf{F}_i$ is the dynamic coefficient matrix for spacecraft i, which can be separated since the equations of motion for each spacecraft are uncoupled. It is important to note here the distinction between $\mathbf{F}_i$ and $\mathbf{F}_k$: $\mathbf{F}_i$ is a sub-matrix of $\mathbf{F}$, while $\mathbf{F}_k$ is simple $\mathbf{F}$ evaluated at the discrete time t_k.

Similarly, applying the definition for the measurement sensitivity matrix ($\mathbf{H}$) to Eqs. (4) and (5) results in

$$\frac{\partial \rho_{ji}}{\partial \mathbf{r}_i} = \frac{\boldsymbol{\rho}_{ji}{}^T}{\rho_{ji}} \quad , \quad \frac{\partial r_{ij}}{\partial \mathbf{r}_i} = -\frac{\mathbf{r}_{ij}{}^T}{r_{ij}} \quad , \quad \frac{\partial r_{ij}}{\partial \mathbf{r}_j} = +\frac{\mathbf{r}_{ij}{}^T}{r_{ij}} \tag{10}$$

while all remaining partial derivatives are equal to zero.

C. State Estimate and Error Covariance Propagation

After initialization, as described in Eq. (6), the state estimate vector and state error covariance matrix are propagated using Eq. (11).

$$\dot{\hat{\mathbf{x}}}(t) = \mathbf{f}(\hat{\mathbf{x}}(t), t) \quad , \quad \mathbf{P}_{k+1}(-) = \boldsymbol{\Phi}_k\mathbf{P}_k(+)\boldsymbol{\Phi}_k^T + \mathbf{Q}_k \tag{11}$$

The state transition matrix ($\boldsymbol{\Phi}$) and the process noise covariance matrix ($\mathbf{Q}$) are propagated simultaneously with $\mathbf{P}$ using Eqs. (12) and (13), respectively.

$$\dot{\boldsymbol{\Phi}}_k = \mathbf{F}_k\boldsymbol{\Phi}_k, \quad , \quad \boldsymbol{\Phi}_k \equiv \boldsymbol{\Phi}(t_{k+1}, t_k) \quad , \quad \boldsymbol{\Phi}_0 = \mathbf{I} \tag{12}$$

$$\dot{\mathbf{Q}}_k = \mathbf{F}_k\mathbf{Q}_k + \mathbf{Q}_k\mathbf{F}_k^T + \mathbf{Q}_{spec} \quad , \quad \mathbf{Q}_0 = \mathbf{0} \tag{13}$$

D. State Estimate and Error Covariance Update

The state estimate and error covariance are propagated until a measurement becomes available at time t_k. At which time the state estimate is updated with the product of the Kalman gain matrix ($\mathbf{K}$),

$$\mathbf{K}_k = \mathbf{P}_k(-)\mathbf{H}_k^T\underbrace{\left[\mathbf{H}_k\mathbf{P}_k(-)\mathbf{H}_k^T + \mathbf{R}_k\right]^{-1}}_{\mathbf{W}_k} \tag{14}$$

and the measurement residual, as seen in Eq. (15).

$$\hat{\mathbf{x}}_k(+) = \hat{\mathbf{x}}_k(-) + \mathbf{K}_k\left[\mathbf{z}_k - \mathbf{h}_k(\hat{\mathbf{x}}_k(-))\right] \tag{15}$$

The measurement residual is the difference between the measurement and the measurement model evaluated at the *pre*-updated state estimate and has residual covariance $\mathbf{W}$. At this time the error covariance is also updated. The error covariance is updated using the numerically stable Joseph formulation:

$$\mathbf{P}_k(+) = (\mathbf{I} - \mathbf{K}_k\mathbf{H}_k)\mathbf{P}_k(-)(\mathbf{I} - \mathbf{K}_k\mathbf{H}_k)^T + \mathbf{K}_k\mathbf{R}_k\mathbf{K}_k^T. \tag{16}$$

To ensure that the error covariance is still symmetric after the update, $\mathbf{P}$ is added to its transpose and divided by two ($\mathbf{P} = (\mathbf{P} + \mathbf{P}^T)/2$).

Equations (15) and (16) show the matrix form of the update, which process all m measurements for a given time at once. Alternatively the measurements for a given time can be processed one by one. This is done by using the corresponding row of $\mathbf{H}$ and diagonal element of $\mathbf{R}$ in place of the full matrices. Consequently *only the corresponding diagonal element of* $\mathbf{W}$ *is used* and $\mathbf{K}$ becomes a vector. After each measurement is processed $\mathbf{h}$ and $\mathbf{H}$ must be reevaluated using the new (recently updated) $\hat{\mathbf{x}}$ and $\mathbf{P}$. This procedure is repeated until all m measurements have been processed. Although this method is more computationally stable, it inherently causes the order in which measurements are processed to become significant.

III. Observability Condition

The linear time-invariant observability matrix is defined as

$$\mathbf{O} = \left[\begin{array}{ccccc} \mathbf{H}^T & (\mathbf{HF})^T & (\mathbf{HF}^2)^T & \cdots & (\mathbf{HF}^{n-1})^T \end{array} \right]^T_{nm \times n} \tag{17}$$

where n is the length of the state vector ($\mathbf{x}$) and m is the length of the measurement and measurement model vectors ($\mathbf{z}$ and $\mathbf{h}$ respectively). The matrices $\mathbf{F}$ and $\mathbf{H}$ are defined by Eq. (7) (but evaluated at $\mathbf{x}$).

The observability condition for a continuous deterministic n^{th}-order, linear time-invariant system is that the system is observable if, and only if, matrix $\mathbf{O}$ has rank n (which is equivalent to $\mathbf{O}$ having n linearly independent rows). Furthermore, $\mathbf{O}$ has rank n if, and only if, for $m = 1$, $\det(\mathbf{O}) \neq 0$ and for $m > 1$, $\det(\mathbf{O}^T\mathbf{O}) \neq 0$.[2]

Although the systems examined in this paper are neither linear nor time-invariant, examination of this observability condition still provides useful insight into the overall observability of the systems (our ability to determine the state from the measurements). For this reason, within the context of this paper the terms "observable," "observability," and "observability matrix" refer to the framework of the aforementioned observability condition (unless explicitly stated otherwise).

IV. Simulations Results

Using the equations developed in Section II, three simulations were examined. The first simulation, a simple two-dimensional (2-D) problem, investigates the observability and navigation issues of one spacecraft travelling in the Earth-Moon vicinity. In the second simulation the problem is expanded to three dimensions (3-D) and a second spacecraft is added to examine the effect of the addition of a relative (cross-link) range measurement between spacecraft. Finally, the third simulation adds four more spacecraft to study the observability and navigation behavior when multiple cross-link measurements are used.

The first simulation uses an Earth-centered inertial (ECI) frame (i.e. body 1 = Earth) with a free-return trajectory, while the second and third simulations use a Moon-centered inertial (MCI) frame (i.e. body 1 = Moon) with spacecraft in low lunar orbits. Both frames are orientated such that the Earth-Moon line is initially along the X-axis and the bodies orbit plane is the X-Y plane.

The following guidelines or methods apply to all three simulations. First, to ensure observability the number of tracking stations used is always equal to the dimension of space in the problem (e.g. 2 stations in 2-D, 3 stations in 3-D). The tracking stations, which are located at libration points, are assumed to be known exactly and assumed to have constant visibility of the spacecraft. Next, the row-by-row update was chosen because the matrix form was found to be overly sensitive when processing relative range measurements. In addition, because of this sensitivity, *all tracking station range measurements are always processed before any cross-link range measurements*. Finally, to simplify filter tuning in this preliminary study, identical dynamics were used in the filter and the simulated environment. Consequently, process noise was typically not used ($\mathbf{Q}_{spec} = \mathbf{0}$). Similarly, unless otherwise stated, the measurement noise covariance used in the filter is identical to that used in the simulated environment. Finally, to avoid potential numerical problems the same measurement noise covariance is used for all measurements, both tracking station ranges and cross-link ranges.

A. Simulation 1: 1 Spacecraft in 2-D

In Simulation 1 one spacecraft is tracked in 2-D ($n = 4$) using two tracking stations ($m = 2$) located at each of the two equilateral libration points (L4 and L5). The measurement vector, measurement sensitivity matrix, and observability matrix can then be assembled using Eqs. (4), (7-10), and (17), as seen in Eq. (18).

$$\mathbf{h} = \begin{bmatrix} \rho_1 \\ \rho_2 \end{bmatrix} \quad , \quad \mathbf{H} = \begin{bmatrix} \boldsymbol{\rho_1}^T/\rho_1 & \mathbf{0}^T \\ \boldsymbol{\rho_2}^T/\rho_2 & \mathbf{0}^T \end{bmatrix} \quad , \quad \mathbf{O} = \begin{bmatrix} \boldsymbol{\rho_1}^T/\rho_1 & \mathbf{0}^T \\ \boldsymbol{\rho_2}^T/\rho_2 & \mathbf{0}^T \\ \mathbf{0}^T & \boldsymbol{\rho_1}^T/\rho_1 \\ \mathbf{0}^T & \boldsymbol{\rho_2}^T/\rho_2 \\ \boldsymbol{\rho_1}^T\mathbf{G}/\rho_1 & \mathbf{0}^T \\ \boldsymbol{\rho_2}^T\mathbf{G}/\rho_2 & \mathbf{0}^T \\ \mathbf{0}^T & \boldsymbol{\rho_1}^T\mathbf{G}/\rho_1 \\ \mathbf{0}^T & \boldsymbol{\rho_2}^T\mathbf{G}/\rho_2 \end{bmatrix} \tag{18}$$

(Since there is only one spacecraft, the i subscript has been dropped for convenience.) At this point it should be noted that the terms containing $\mathbf{G}$ are relatively small. In fact, at best (very close to the bodies) $\|\mathbf{G}\|$ is of order 10^{-6} while during most the trajectory the order of $\|\mathbf{G}\|$ is closer to 10^{-10} (with a minimum order of 10^{-11}). Consequently, for simplification these terms will be considered $\mathbf{0}^T$.[*] Since $n = 4$, this implies that the remaining four rows must all be linearly independent in order to satisfy the observability condition. However, by examining $\mathbf{O}$ we see that if $\boldsymbol{\rho_1}$ and $\boldsymbol{\rho_2}$ are parallel the number of linearly independent rows is reduced to two and thus the observability condition is violated.

This can be illustrated both numerically and geometrically. Numerically this can be detected by computing the determinant of $\mathbf{O}^T\mathbf{O}$. Recall that the observability condition is violated when $\det(\mathbf{O}^T\mathbf{O}) = 0$. Geometrically this violation occurs when the spacecraft crosses a line connecting the two tracking stations. Figure 1 illustrates the detection of these events. In Figure 1(b) the light-blue dot at (0,0) represents the

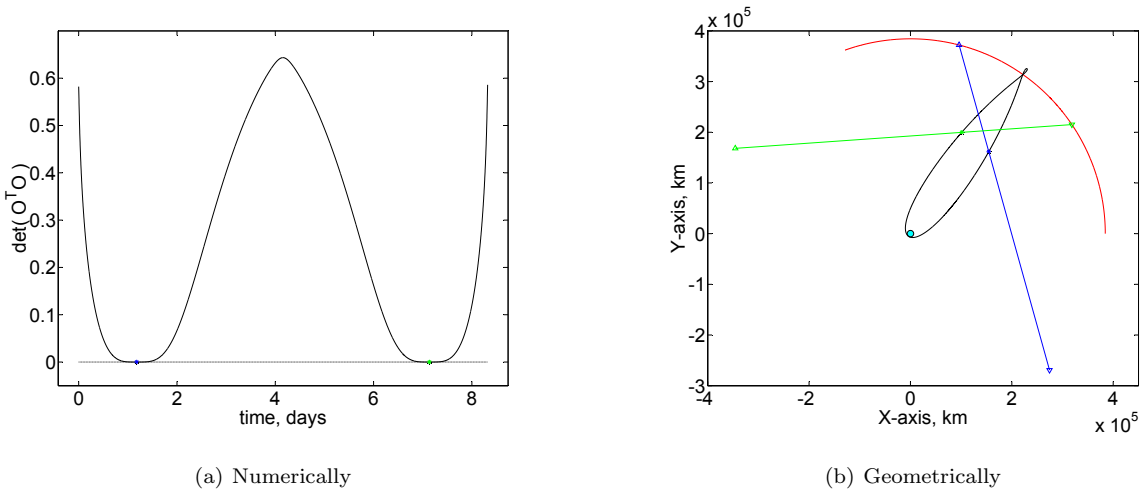(a) Numerically

(b) Geometrically

Figure 1. In (a) and (b) the blue and green markings denote events occurring at the same respective times. The times where the blue and green points occur in (a) have been marked on the black trajectory in (b). At these times a line connects the L4 tracking station (denoted by a triangle) and the L5 tracking station (denoted by an upsidedown triangle), indicating that both range vectors are parallel.

---

[*]This simplification is not made when computing $\det(\mathbf{O}^T\mathbf{O})$ numerically.

Earth while the red arc represents the trajectory of the Moon. The free-return trajectory is displayed in black. The spacecraft begins near the Earth, encounters the Moon, and then return to the Earth.

The state was then estimated using the algorithms presented in Section II. The state estimate was initialized by adding an uncertainty (noise) with a standard deviation of 1000 m in position and 1 m/s in velocity to the initial true state. Measurements were taken simultaneously from both tracking stations at equal time intervals of approximately 1 hour. The noise on both range measurements had a standard deviation of 1 m. Figure 2 shows that, as expected, the residuals appear to be white noise with a standard deviation of about 1 m.

The navigation state error can be seen in Figure 3. Notice that the bulges in covariance occurring around 1.2 days coincide with the first violation of the observability condition, as seen in Figure 1(a). Next, around 4.2 days the velocity covariance begins to bulge again. Although this occurs when $\det(\mathbf{O}^T\mathbf{O})$ is furthest from zero, it should be noted that at this time the spacecraft is in the lunar flyby portion of the trajectory; hence the changes in velocity are at a climax. Similarly, the bulges in covariance at the end

Figure 2. Time history of the range residuals (blue) and the square root of the corresponding residual covariances (red).

of the time history are due to the return flyby of the Earth. Once through this portion of the trajectory the state errors and covariances begin to converge once more.
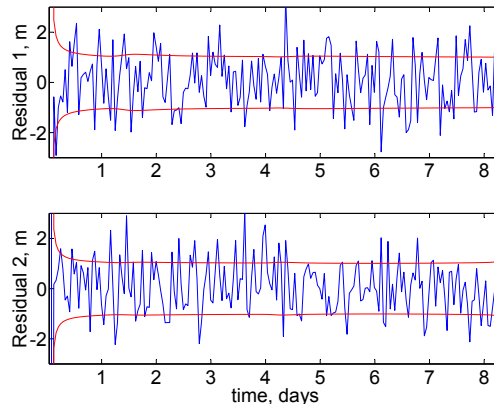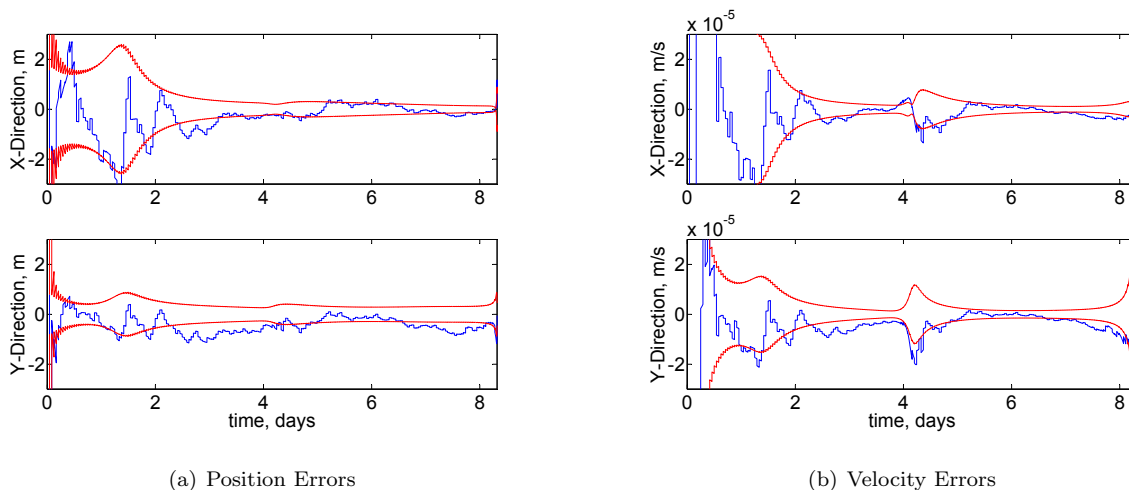

(a) Position Errors

(b) Velocity Errors

Figure 3. Time history of the state errors (blue) and the square root of the corresponding error covariances (red).

This simple simulation has shown that examination of the observability condition can help detect potential problems in the state navigation. In particular the 2-D system becomes unobservable when range vectors are parallel. Simulation 2 extends this concept into 3-D while also examining the advantages and concerns of adding a second spacecraft.

B. Simulation 2: 2 Spacecraft in 3-D

Simulation 2 consists of two parts, a and b. In Simulation 2a two spacecraft are tracked in 3-D ($n = 12$) using three tracking stations ($m = 6$): two located at each of the equilateral libration points (L4 and L5) and one at the co-linear libration point on the far-side of the Moon (L2). Simulation 2b is identical to Simulation 2a with one exception, the addition of 1 cross-link range measurement ($m = 7$). Using Eqs. (4-5) and (10) the measurement vector and measurement sensitivity matrix for Simulation 2b then become

$$\mathbf{h} = \begin{bmatrix} \rho_{11} \\ \rho_{21} \\ \rho_{31} \\ \rho_{12} \\ \rho_{22} \\ \rho_{32} \\ r_{12} \end{bmatrix} \quad \text{and} \quad \mathbf{H} = \begin{bmatrix} \boldsymbol{\rho}_{11}{}^T/\rho_{11} & \mathbf{0}^T & \mathbf{0}^T & \mathbf{0}^T \\ \boldsymbol{\rho}_{21}{}^T/\rho_{21} & \mathbf{0}^T & \mathbf{0}^T & \mathbf{0}^T \\ \boldsymbol{\rho}_{31}{}^T/\rho_{31} & \mathbf{0}^T & \mathbf{0}^T & \mathbf{0}^T \\ \mathbf{0}^T & \mathbf{0}^T & \boldsymbol{\rho}_{12}{}^T/\rho_{12} & \mathbf{0}^T \\ \mathbf{0}^T & \mathbf{0}^T & \boldsymbol{\rho}_{22}{}^T/\rho_{22} & \mathbf{0}^T \\ \mathbf{0}^T & \mathbf{0}^T & \boldsymbol{\rho}_{32}{}^T/\rho_{32} & \mathbf{0}^T \\ -\mathbf{r}_{12}{}^T/r_{12} & \mathbf{0}^T & \mathbf{r}_{12}{}^T/r_{12} & \mathbf{0}^T \end{bmatrix} \tag{19}$$

respectively. (The measurement vector and measurement sensitivity matrix for Simulation 2a can easily be obtained from Eq. (19) by removing rows containing cross-link range terms.) Due to its size the observability matrix will not be presented here. However, once again it should be noted that the terms containing $\mathbf{G}$ are relatively small. Although, since the spacecraft remain close to the Moon the order of $\|\mathbf{G}\|$ remains around 10^{-6}, due to the increased dimension of the state, the observability matrix now contains powers of $\mathbf{G}$ which causes exceptionally small terms. Consequently, for simplification these terms will again be considered $\mathbf{0}^T$ and the observability matrix essentially only contains the terms $\mathbf{H}$ and $\mathbf{HF}$.

First let us examine the terms $\mathbf{H}$ and $\mathbf{HF}$ assuming cross-link ranges are not being used. Once again we see that if any tracking station range vectors to the *same*[†] spacecraft are parallel, the corresponding set of rows of the observability matrix is linearly dependent. This implies that the set contributes only one linearly independent row. With the addition of a third tracking station this result can be extended even further. Since any two linearly independent vectors in $\mathcal{R}^3$ form the basis for a plane, any other vector that lies in this plane is linearly dependent on the basis vectors.[3] Consequently, if three or more tracking station range vectors to the same spacecraft lie in the same plane, the corresponding set of rows of the observability matrix is linearly dependent. This implies that the set contributes only two linearly independent rows.

Now let us reexamine the terms $\mathbf{H}$ and $\mathbf{HF}$ with the addition of cross-link range. We now notice that if any tracking station range vectors to two *different*[‡] spacecraft are parallel, and the cross-link range vector between these two spacecraft is also parallel, then the corresponding set of rows of the observability matrix is linearly dependent. This implies that this set of three contributes only two linearly independent rows. In other words this particular cross-link measurement is not contributing towards the observability of the state. This result can also be extended. Suppose that tracking station range vectors from two stations to one spacecraft form a plane; and, two more tracking station range vectors to a different spacecraft form another plane. If the two planes are coplanar the cross-link range vector between these two spacecraft must also lie in this plane because it has a point in each plane (located at each spacecraft); therefore, the corresponding set of rows of the observability matrix is linearly dependent. Similarly, if these two planes are not coplanar, but the cross-link range vector between these two spacecraft lies along the intersection of these two planes, then the corresponding set of rows of the observability matrix is again linearly dependent. In both instances the set of five contributes only four linearly independent rows. Once again this implies that this particular cross-link measurement is not contributing towards the observability of the state.

[†]The tracking station range vectors must be to the same spacecraft because tracking station range terms for different spacecraft are contained in different columns of the observability matrix; consequently rows involving different spacecraft are always linearly independent.

[‡]The tracking station range vectors must now be to two different spacecraft because cross-link range (between these two spacecraft) terms occur in the same columns of the observability matrix as the tracking station range terms of the two spacecraft; consequently two different spacecraft are required in order to span the columns of the rows containing cross-link range terms.

Figure 4 illustrates the detection of these events both numerically and geometrically. However, although the detection of these events may cause drop-offs in observability, they do not necessarily indicate a complete loss of observability (i.e. the number of linearly independent rows of the observability matrix may still be n). This is especially important to remember considering the simplification made that rows containing $\mathbf{G}$ are negligible. This simplification is not made when computing $\det(\mathbf{O}^T\mathbf{O})$ numerically. Recall that all three
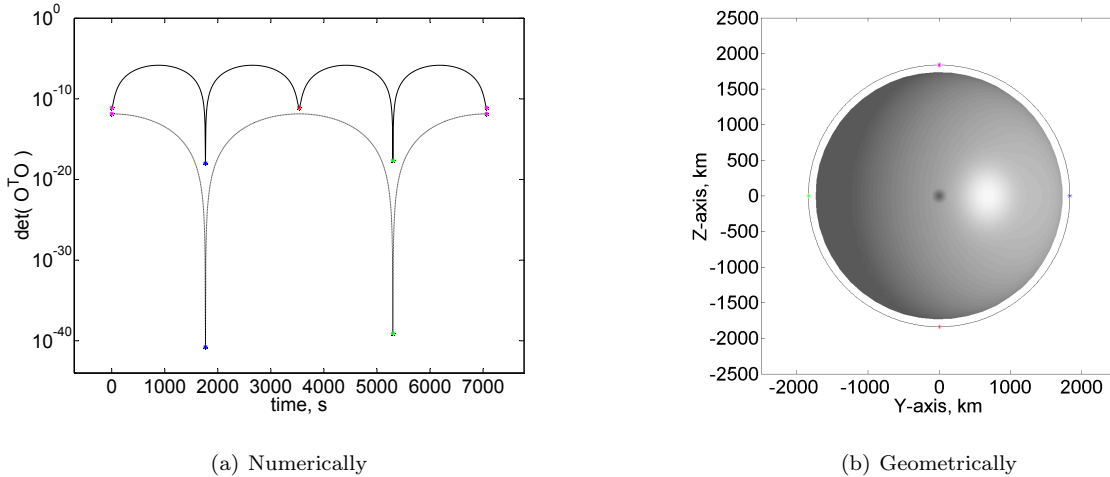

(a) Numerically

(b) Geometrically

Figure 4. In (a) and (b) the colored points denote events occurring at the same respective times. The times where the colored points occur in (a) have been marked on the black trajectory in (b). In (b), the lower curve is for Simulation 2a while the upper curve is for Simulation 2b.

tracking stations lie in the same plane (X-Y plane). If the trajectory of the spacecraft also remained in the X-Y plane all range vectors would lie in the same plane for all time and the observability condition would be violated for all time. For this reason a trajectory perpendicular to the X-Y plane was chosen. Both spacecraft were placed in the same circular orbit (in the Y-Z plane) with the second spacecraft trailing such that its initial range from the first spacecraft was 1 km. Despite the chosen trajectory, there are still two points of concern. First, as seen in Figure 4 at times 1767 s and 5300 s, there is still a considerable drop-off in observability when the trajectory crosses the X-Y plane. Second, since the tracking stations are far away relative to the amount that the trajectory goes out of plane, the tracking station range vectors still nearly lie in the same plane. Consequently, the value of $\det(\mathbf{O}^T\mathbf{O})$ remains small relative to that of Simulation 1.

That being said Figure 4(a) still illustrates the increase in observability due to the addition of a cross-link measurement. Notice that when the cross-link is included $\det(\mathbf{O}^T\mathbf{O})$ is always greater than it is without the cross-link included. Also, notice that near times 0 s, 3534 s, and 7067 s the $\det(\mathbf{O}^T\mathbf{O})$ for both Simulation 2a and 2b is approximately the same. This is expected because one of the aforementioned events occurs at these times. In particular the planes created by the tracking station range vectors to two spacecraft are coplanar. In order to visualize this we will review the geometry of the problem at these times. First, notice that these events occur when both spacecraft are near the "top" and "bottom" of the orbit. To be more exact, the the cross-link range vector between the two spacecraft is parallel with the Y-axis; which more importantly, is also parallel with a line connecting the L4 and L5 tracking stations. This implies that the plane created by the L4 and L5 tracking station range vector to the first spacecraft is coplanar with the plane created by the L4 and L5 tracking station range vector to the second spacecraft. Therefore, as described earlier, the cross-link row in the observability matrix is merely a linear combination of the four tracking station rows. Consequently, the cross-link measurement contributes no additional information and Simulation 2b is reduced to Simulation 2a.

The state was then estimated using the algorithms presented in Section II. The state estimate was initial-

ized by adding an uncertainty (noise) with a standard deviation of 1000 m in position and 1 m/s in velocity to the initial true state. Simulation 2a and Simulation 2b used identical initial state estimates. Measurements were taken simultaneously from all tracking stations (as well as between spacecraft for Simulation 2b) at equal time intervals of approximately 1 minute. The noise on all range measurements (including cross-links for Simulation 2b) had a standard deviation of 1 m. As expected all residuals appeared to be white noise with a standard deviation of about 1 m, similar to what was seen in Figure 2.

The navigation state error for one spacecraft in Simulation 2a, can be seen in Figure 5. Plots for

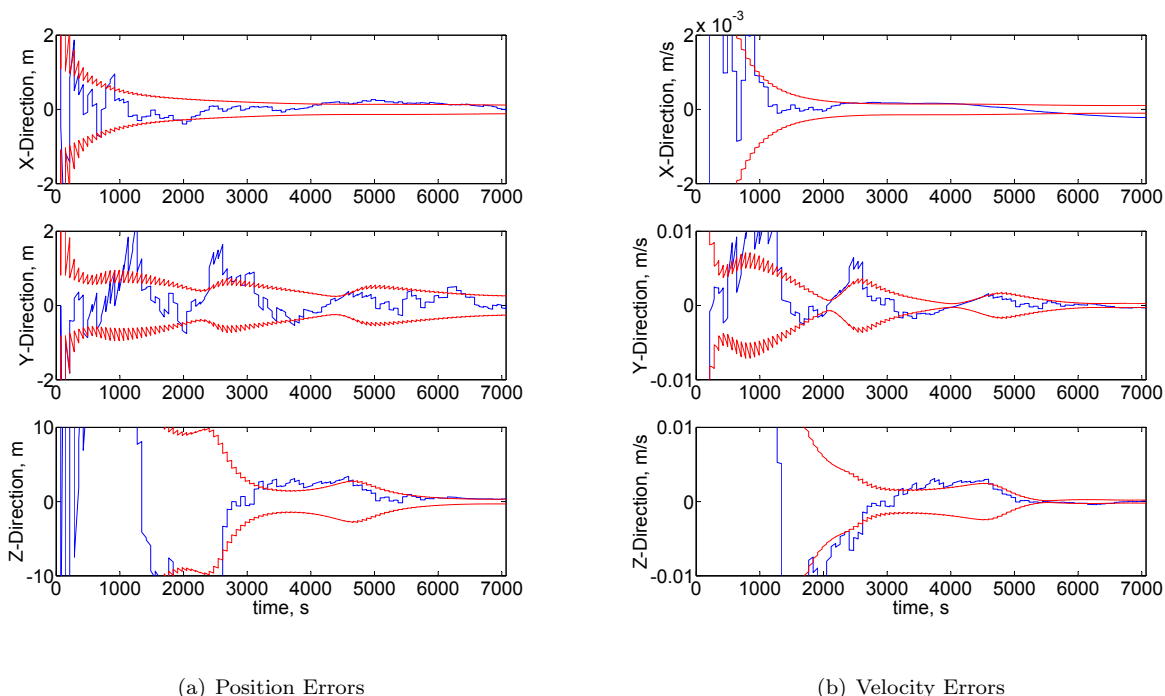(a) Position Errors   (b) Velocity Errors

Figure 5. Time history of the state errors (blue) and the square root of the corresponding error covariances (red) for one spacecraft in Simulation 2a.

Simulation 2b and the second spacecraft will not be presented here as they look very similar to Figure 5. In fact, the plots look so similar it is difficult to see the advantage of using the cross-link measurement. However, by examining the error covariance that bounds the state error at the final time for Simulation 2a and Simulation 2b, we do see a slight reduction in navigation error (see Table 1). The reduction in navigation error is small because only one cross-link measurement is available. Furthermore, notice in Table 1 that there is no change in the components in the X-direction. This is because all cross-link range measurement are in the Y-Z plane and therefore do not contribute any information about the X-direction.

This simulation has illustrated how the geometry of a problem can affect observability. It has also demonstrated that relative measurements can be used to decrease inertial navigation error. Simulation 3 extends this concept further by examining the advantages and concerns of using multiple cross-link measurements.

C. Simulation 3: 6 Spacecraft in 3-D

Simulation 3 also consists of two parts, a and b. In Simulation 3a six spacecraft are tracked in 3-D ($n = 36$) using three tracking stations ($m = 18$): two located at each of the equilateral libration points (L4 and L5) and one at the co-linear libration point on the far-side of the Moon (L2). Simulation 3b is identical to Simulation

3a with one exception, the addition of 15 cross-link range measurements ($m = 33$). The measurement vector for Simulation 3b can be composed using Eqs. (4-5); however, due to its size it is presented in Eq. (20) in a condensed form.

$$\mathbf{h} = \begin{bmatrix} \rho_{11} & \dots & \rho_{36} & r_{12} & \dots & r_{56} \end{bmatrix}^T \tag{20}$$

(The measurement vector for Simulation 3a can easily be obtained from Eq. (20) by removing rows containing cross-link range terms.) The measurement sensitivity matrix and the observability matrix are too large to present here. However, the observability matrix shares all of the reduced observability events presented in Section IVB. Furthermore, due to the size of $\mathbf{G}$ for simplification these terms will again be considered $\mathbf{0}^T$ and the observability matrix essentially only contains the terms $\mathbf{H}$ and $\mathbf{HF}$.

By examining $\mathbf{H}$ we see that the addition of multiple cross-link measurements yields an additional reduced observability event. In particular, consider the rows containing cross-link terms between any three spacecraft. If any two cross-link range vectors between these three spacecraft are parallel, the third must also be parallel (i.e. the spacecraft are collinear). Consequently, the corresponding set of rows of the observability matrix is linearly dependent. Therefore this set of three contributes only two linearly independent rows, which implies that one of the cross-link measurements is not contributing towards the observability of the state.

While the orbits and orientation of the spacecraft in Simulation 3 were chosen such that this event does not occur, the events and concerns described in Section IVB still do occur. The numerical detection of those events are illustrated in Figure 6 while Figure 4(b) is still valid for the geometrical detection. The trajectory of the first two spacecraft is the same as what was used in Simulation 2. Two more orbit planes were created by tilting the original orbit 1 km from the Y-Z plane in both directions. Two spacecraft were placed in each plane with one spacecraft trailing such that its initial range from the other spacecraft was 1 km. The six spacecraft were then orientated in their respective planes such that they remained nearby (0.5-2.5 km). Consequently, since the spacecraft are so close in the orbit planes and the planes are nearly coplanar, Figure 4(b) is still valid for Simulation 3.

Figure 6 illustrates the drastic increase in observability due to the cross-link measurements. Notice that the addition of multiple cross-links compensates for the loss of observability during the X-Y plane crossing. Also, while reductions in observability still do occur near the "top" and "bottom" of the orbits, as in Simulation 2, Simulation 3b is never fully reduced to Simulation 3a because of the use of multiple cross-links.

Figure 6. Numerical detection. The lower curve is for Simulation 3a while the upper curve is for Simulation 3b.

Once again, the state was then estimated using the algorithms presented in Section II. The state estimate was initialized by adding an uncertainty (noise) with a standard deviation of 1000 m in position and 1 m/s in velocity to the initial true state. Simulation 3a and Simulation 3b used identical initial state estimates. Measurements were taken simultaneously from all tracking stations (as well as between spacecraft for Simulation 3b) at equal time intervals of approximately 1 minute. The noise on all range measurements (including cross-links for Simulation 3b) had a standard deviation of 1 m. As expected all residuals appeared to be white noise with a standard deviation of about 1 m, similar to what was seen in Figure 2.

The navigation state error plots for Simulation 3a will not be presented here as it looked very similar to what was seen in Figure 5. In fact, as seen in Table 1, the average of the final error covariance for all six spacecraft for Simulation 3a was the same as Simulation 2a. However, reduction in navigation state error
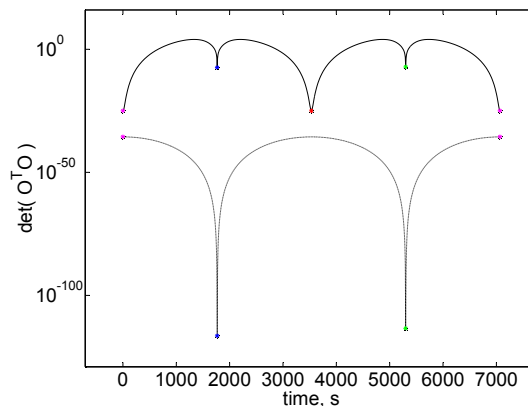
for Simulation 3b is quite noticeable. As seen in Figure 7, there appears to be an increase in the rate of convergence, especially in the Z-position and Y-velocity. Likewise, as seen in Table 1, not only is there a

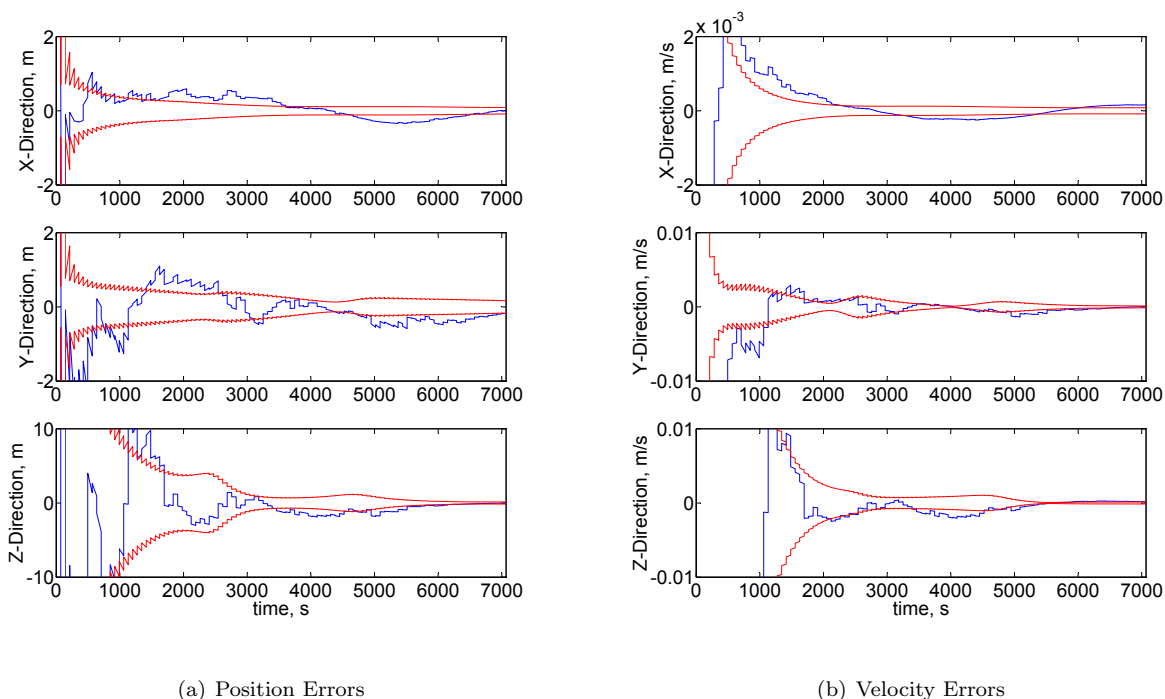(a) Position Errors

(b) Velocity Errors

Figure 7. Time history of the state errors (blue) and the square root of the corresponding error covariances (red) for one spacecraft in Simulation 3b.

considerable reduction in the final error covariance for Simulation 3b, but unlike Simulation 2b, this reduction includes the X-direction. The reduction in the X-direction is the direct result of cross-link measurements taken out of the Y-Z plane

Table 1. State error covariance comparison. The values shown are the average values of all the spacecraft.

$(t = t_f)$	$P_{xx}^{1/2}$, m	$P_{yy}^{1/2}$, m	$P_{zz}^{1/2}$, m	$P_{\dot{x}\dot{x}}^{1/2}$, m/s	$P_{\dot{y}\dot{y}}^{1/2}$, m/s	$P_{\dot{z}\dot{z}}^{1/2}$, m/s
Sim. 2a	0.116	0.252	0.317	1.03×10^{-4}	2.69×10^{-4}	2.10×10^{-4}
Sim. 3a	0.116	0.252	0.317	1.03×10^{-4}	2.69×10^{-4}	2.10×10^{-4}
Sim. 2b	0.116	0.212	0.233	1.03×10^{-4}	1.96×10^{-4}	1.76×10^{-4}
Sim. 3b	0.0788	0.173	0.147	0.765×10^{-4}	1.22×10^{-4}	1.43×10^{-4}

V.   Conclusion

This paper has examined the advantages and concerns associated with the use of combinations of inertial and relative measurements. During the research the following observations and conclusions were made in regard to the navigation algorithms presented in Section II:

- *row-by-row update appears to be more stable than matrix form when using relative measurements*

- *order measurements are processed matters (process all inertial measurements first)*

- *different measurement noise for relative and inertial measurements may cause instability*

Adhering to these guidelines we considered the impact of trajectory geometry on observability. Using the observability condition outlined in Section III, Section IVA and IVB examined possible reductions in observability when using (inertial) tracking station range measurements due to the following geometric anomalies:

- *1 spacecraft and the 2 or more stations tracking it are collinear*

- *1 spacecraft and the 3 or more stations tracking it are coplanar*

Sections IVB and IVC expanded these results to include the use of (relative) cross-link range measurements and presented the following additional geometric anomalies:

- *2 spacecraft and the station(s) tracking each are collinear*

- *the line connecting 2 spacecraft is parallel to the line connecting the 2 stations tracking each spacecraft*

- *3 spacecraft are collinear*

It was shown in both Simulation 2 and 3 that the use of relative measurements can directly contribute to the observability of the inertial state and consequently improve the state estimate.

Although not presented in this paper, supplementary work included the use of tracking station range-rate measurements and an analysis of the non-linear observability matrix (within the context of Simulation 1). In the framework of Section III, range-rate measurements ($\dot{\rho}_{ji}$) were found to produce similar geometric anomalies to those seen in Simulation 1. For example, the corresponding set of rows of the observability matrix is linearly dependent when the tracking station range-rate vector is parallel to the tracking station range vector. Furthermore, when only using tracking station range measurements the non-linear observability matrix was found to be numerically equivalent to the linear observability matrix to an order of 10^{-5}; however, these matrices become noticeably different with the addition of range-rate measurements.

While the the non-linear time-invariant observability analysis presented in this paper provides useful insight, it by no means exhausts the analysis of the problem. Mixing relative measurements with inertial measurements can be extremely delicate due to numerical instabilities. Additional work is necessary to uncover the finer points of using relative measurements for inertial navigation. In particular, reexamination of the non-linear observability matrix with the addition of relative range measurements, as well as the examination of the time varying observability Gramian, may provide a more complete understanding of the problem.

Acknowledgments

References

[1]Gelb, A., *Applied Optimal Estimation*, The M.I.T. Press, Cambridge, MA, 1974.

[2]Chen, C. T., *Linear System Theory and Design*, Oxford University Press, New York, 1999.

[3]Lay, D. C., *Linear Algebra and Its Applications*, Addison Wesley, Boston, 2003.